Numerical Study of Extension-Thinning Inelastic Fluid Flow: Galerkin Finite Element Method

Ahmed J. Ghanim*, Alaa H. Al-Muslimawi

Department of Mathematics, College of Science, University of Basrah, Basra, Iraq

*Corresponding author E-mail: pgs.ahmed.jameel@uobasrah.edu.iq

https://doi.org/10.29072/basjs.20250104

ARTICLE INFO

Keywords

Artificial compressibility method; Finite element method; Galerkin method; Navier-Stokes; Non-Newtonian fluids.

ABSTRACT

In the current investigation, the simulation of extension-thinning inelastic fluid flow is considered through an axisymmetric rectangular channel. To describe the fluid motion, usually, the mass conservation and conservation of momentum partial differential equations are used. This study presents these equations in the context of the cylindrical coordinate system. The key point here is that viscosity needs to be defined as a variable, which requires introducing an additional constitutive equation. Accordingly, an extension-thinning inelastic model, named SI-Fit-II, for treating the viscosity condition is presented.Numerically, the Galerkin finite element approach based on the artificial compression method (AC-method) is performed in this study. To meet the method analysis, Poiseuille flow along a circular channel under an isothermal state is used as a simple test problem. This test is conducted by taking a circular section of the pipe. The influence of many parameters, such as the consistency parameter and power index of the model, the artificial compressibility parameter (βac) and Reynolds number (Re) was discussed. This test is conducted by taking a circular section of the pipe.

Received 09 Dec 2024; Received in revised form 30 Jan 2025; Accepted 13 Feb 2025, Published 30 Apr 2025

1. Introduction

Non-Newtonian fluids are essential to many chemical and industrial operations in the food, metallurgical, polymer, and biological sectors. This kind of fluid reacts to stimuli by changing its viscosity. Consequently, a simple constitutive equation is used to characterize the viscosity of such a fluid. Typical constitutive models that demonstrate non-Newtonian behavior include the power law model (*PLM*), modified power law, cross model, Herschel–Bulkley model, Caro model, Caro–Yasuda model, Baird–Caro model, modified Casson model, and tethering model [1-5]. Furthermore, non-Newtonian fluids show either shear thickening, that is, the process by which viscosity rises as shear increases, or shear thinning, in which the viscosity falls as shear increases.

In this study, the flow of inelastic fluids was studied extensively, using an inelastic extensional model called Fit-II. This model represents one of the fundamental constitutive equations for such fluids (for more details, see Binding et al. [6] and Debbaut and Crochet [7]). The definition of such a model with extensional response is

$$\mu_E(\dot{\varepsilon}) = 3\mu_0\, cosh(n\lambda\dot{\varepsilon}).(1+3(k\dot{\varepsilon})^2)^{(n-1)/2},$$

where n, λ, and k are the parameters in the model that determine the extensional behaviors of the model, and μ_0 indicates the zero viscosity (for more details see [6-8]). Generally, from the structure of this model, one can see that the functions of viscosity are presented for extensional flows only.

The material behavior in these types of flows, which is described by a combination of governing equations and the Fit-II model, represents a complicated problem. Thus, the numerical treatment is the essential tool to analyze this problem. Accordingly, several numerical studies have been conducted on such inelastic models, see for example, [6],[7], and [9]. These investigations show how extensive the information to researchers interested in this type of flow.

In this study, we introduced a robust numerical algorithm to treat the governing equations that describe this flow. This numerical approach is performed by using the Galerkin finite element method based on the artificial compression method (*AC*-method), for short, it is called *GFE-AC*-method. The main idea of *AC*-method is to transform the continuity equation from an elliptic equation to a hyperbolic equation by adding the artificial compressibility term, as will be explained later. Then, the resulting system can be solved directly by standard time-dependent approaches that are not complicated to apply in the solution. Chorin (1967) is the first person who adopted this method to solve the Navier-Stokes equations [10]. Later, this method has also been applied for solving unsteady problems (see, for example, Peyret and Taylor [11] and Kao and Yang [12]).

Moreover, one can view different studies of the *AC*-method that were conducted by combining this method with finite element and finite difference methods (see, for example, [11-16]).

The main novelty in this research is the study of inelastic axisymmetric and laminar extensional fluid flow by using *GFE-AC*-method, which none of the researchers have previously shed light on. The effect of Reynolds number (*Re*) and all the parameters of the Fit-II model on the fluid behavior is presented as well. To test our algorithm, the Poiseuille (*Ps*) flow through a two-dimensional straight channel, under isothermal conditions, is used as an actual application.

2. Mathematical modeling

2.1 Motion equations

A key formula in fluid mechanics that describes the motion of incompressible fluids is the Navier-Stokes equations. These equations consist of continuity and momentum equations, which are expressed as:

$$\nabla \cdot u = 0, \tag{1}$$

$$\rho \frac{\partial u}{\partial t} = \nabla \cdot (2\mu(\dot{\gamma}, \dot{\varepsilon})d) - \rho(u \cdot \nabla u) - \nabla P. \tag{2}$$

Here, $d = \frac{1}{2}(\nabla u + \nabla u^T)$ is the rate of deformation tensor, P and ρ are the pressure and density of the fluid. The dimensionless Navier-Stokes equations may be expressed using the Reynolds number, a crucial fluid mechanics variable that indicates the ratio of driving forces to viscous forces. The Reynolds number is defined using the following formula: $Re = \frac{\rho UL}{\mu}$, where ρ, L and U are represented by density, length, and velocity, respectively (see [17],[18]). Therefore, the momentum conservation equation (2) can be reformulated as follows:

$$Re \frac{\partial u}{\partial t} = \nabla \cdot (2\mu(\dot{\varepsilon})d) - Re(u \cdot \nabla u) - \nabla P. \tag{3}$$

Furthermore, we convert the continuity equation and the momentum conservation equation into cylindrical coordinates as follows:

$$\frac{\partial u_r}{\partial r} + \frac{1}{r}u_r + \frac{1}{r}\frac{\partial u_\theta}{\partial \theta} + \frac{\partial u_z}{\partial z} = 0. \tag{4}$$

r-direction

$$\frac{\partial u_r}{\partial t} + u_r \frac{\partial u_r}{\partial r} + u_\theta\left(\frac{1}{r}\frac{u_r}{\partial \theta} - \frac{1}{r}u_\theta\right) + u_z \frac{\partial u_r}{\partial z} = \frac{-1}{\rho}\frac{\partial P}{\partial r} + \frac{2\mu_E}{\rho}\frac{\partial^2 u_r}{\partial r^2} +$$
$$\frac{\mu_E}{\rho r^2}\frac{\partial^2 u_r}{\partial \theta^2} - \frac{\mu_E}{\rho r^2}\frac{\partial u_\theta}{\partial \theta} + \frac{2\mu_E}{\rho r}\frac{\partial u_r}{\partial r} + \frac{\mu_E}{\rho r}\frac{\partial^2 u_\theta}{\partial z \partial \theta} + \frac{\mu_E}{\rho}\frac{\partial^2 u_r}{\partial z^2} + \frac{\mu_E}{\rho}\frac{\partial^2 u_z}{\partial z \partial r}. \tag{5}$$

θ - direction

$$\frac{\partial u_\theta}{\partial t} + u_r \frac{\partial u_\theta}{\partial r} + u_\theta \left(\frac{1}{r}u_r - \frac{u_\theta}{\partial \theta}\right) + u_z \frac{\partial u_\theta}{\partial z} = \frac{-1}{\rho r}\frac{\partial P}{\partial \theta} + \frac{2\mu_E}{\rho r^2}\frac{\partial u_r}{\partial \theta} +$$

$$\frac{2\mu_E}{\rho r^2}\frac{\partial^2 u_\theta}{\partial \theta^2} + \frac{\mu_E}{\rho}\frac{\partial^2 u_\theta}{\partial r^2} + \frac{\mu_E}{\rho r}\frac{\partial^2 u_r}{\partial r \partial \theta} + \frac{\mu_E}{\rho}\frac{\partial^2 u_\theta}{\partial z^2} + \frac{\mu_E}{\rho r}\frac{\partial^2 u_z}{\partial z \partial \theta}. \quad (6)$$

z-direction

$$\frac{\partial u_z}{\partial t} + u_r \frac{\partial u_z}{\partial r} + u_\theta \frac{1}{r}\frac{\partial u_z}{\partial \theta} + u_z \frac{\partial u_z}{\partial z} = \frac{-1}{\rho}\frac{\partial P}{\partial z} + \frac{2\mu_s}{\rho}\frac{\partial^2 u_z}{\partial z^2} +$$

$$\frac{\mu_E}{\rho}\frac{\partial^2 u_z}{\partial r^2} + \frac{\mu_E}{\rho r}\frac{\partial u_r}{\partial z} + \frac{\mu_E}{\rho r}\frac{\partial u_z}{\partial r} + \frac{\mu_E}{\rho}\frac{\partial^2 u_r}{\partial r \partial z} + \frac{\mu_E}{\rho r^2}\frac{\partial^2 u_z}{\partial \theta^2} + \frac{\mu_E}{\rho r}\frac{\partial^2 u_\theta}{\partial \theta \partial z}. \quad (7)$$

2.2 Inelastic model

As we mentioned above, the extensional inelastic nonlinear model (Fit-II) is employed to characterize the viscosity behavior for the fluid in the current study. This model may be expressed mathematically as:

$$\mu_E(\dot{\varepsilon}) = 3\mu_0 \cosh(n\lambda\dot{\varepsilon}).(1 + 3(k\dot{\varepsilon})^2)^{(n-1)/2} \quad (8)$$

All the parameters are defined in the introduction above, while here, we need to define the strain rate $\dot{\varepsilon}$ as:

$$\varepsilon^{\cdot} = 3\frac{III_d}{II_d}, \quad (9)$$

Where, II_d and III_d represent the second and third invariants, which are presented in cylindrical coordinates as follows: (see [16])

$$II_d = \frac{1}{2}tr(d^2) = \frac{1}{2}\{(\frac{\partial u_r}{\partial r})^2 + (\frac{\partial u_z}{\partial z})^2 + (\frac{u_r}{r})^2 + \frac{1}{2}(\frac{\partial u_r}{\partial z} + \frac{\partial u_z}{\partial r})^2\}, \quad (10)$$

and

$$III_d = det(d) = \frac{u_r}{r}\left\{\frac{\partial u_r}{\partial r}\frac{\partial u_z}{\partial z} - \frac{1}{4}\left(\frac{\partial u_r}{\partial z} + \frac{\partial u_z}{\partial r}\right)^2\right\}. \quad (11)$$

2.3 Artificial Compressibility Method (*AC*-Method)

The elliptic partial compression equation can be converted into a hyperbolic compressible partial differential form by introducing an artificial component into the continuity equation (4). Once the steady-state solution is reached, the artificial compression term will be removed. The incorporation of this component into the continuity equation can convert the Navier-Stokes equation into a mixed parabolic-hyperbolic equation, which can then be solved using a conventional time-based method. One way to express this approach is to apply the bogus term to the continuity equation.

$$\frac{\partial \rho}{\partial t} + \frac{\partial u_r}{\partial r} + \frac{1}{r}u_r + \frac{1}{r}\frac{\partial u_\theta}{\partial \theta} + \frac{\partial u_z}{\partial z} = 0. \quad (12)$$

The relation between the artificial density and pressure is provided by the state equation that follows:

$$P = \rho\beta_{ac}, \tag{13}$$

where, β_{ac} is the synthetic compressibility parameter; $0 < \frac{1}{\beta_{ac}} << 1$. By replacing Eq. (13) into Eq. (12), we compile the continuity formula in the format:

$$\frac{1}{\beta_{ac}}\frac{\partial P}{\partial t} + \frac{\partial u_r}{\partial r} + \frac{1}{r}u_r + \frac{1}{r}\frac{\partial u_\theta}{\partial \theta} + \frac{\partial u_z}{\partial z} = 0. \tag{14}$$

Therefore, the governing equations for the present study consist of equations (5-7) and (14).

3. Numerical method and test problem

A common numerical method for resolving the partial differential equations in fluid is the Galerkin finite element method. The principal stages of this method are applied to solve equations (5)-(7) and equation (14). The essential step is to find the variational formulation of the governing equations, using suitable weight functions, and compute the integral. After that, we need to define an appropriate interpolation (or shape) function, which is dependent on the number of nodes in the element. Since the element shape in the mesh that we used is a triangle with three vertex nodes and three middle points. Thus, we used a quadratic shape function to approximate the velocity component, while a linear shape function is utilized to approximate the pressure component. These functions can be defined in cylindrical coordinates as:

(a) The quadratic shape function for velocity.

$$\begin{bmatrix}\psi_1\\\psi_2\\\psi_3\\\psi_4\\\psi_5\\\psi_6\end{bmatrix} = \begin{bmatrix}L_1^2 - L_1(L_2+L_3)\\L_2^2 - L_2(L_3+L_1)\\L_3^2 - L_3(L_1+L_2)\\4L_1L_2\\4L_2L_3\\4L_3L_1\end{bmatrix} = \begin{bmatrix}1&0&0&-1&0&-1\\0&1&0&-1&-1&0\\0&0&1&0&-1&-1\\0&0&0&4&0&0\\0&0&0&0&4&0\\0&0&0&0&0&4\end{bmatrix}\begin{bmatrix}L_1^2\\L_2^2\\L_3^2\\L_1L_2\\L_2L_3\\L_3L_1\end{bmatrix}. \tag{15}$$

(b) The linear shape function for pressure

$$\begin{bmatrix}\phi_1\\\phi_2\\\phi_3\end{bmatrix} = \begin{bmatrix}L_1\\L_2\\L_3\end{bmatrix}. \tag{16}$$

Such that, $L_j = \frac{1}{2A_{area}}\left(a_j + b_j r + c_j z\right), \qquad (\forall\, j = 1,2,3)$.

Where, A_{area} is the area of the triangular element, and a_i , b_i and c_i are coefficients. For this, from the divergence theorem and reordering the items, partial differential equations are solved using the weak version of the finite element technique, which involves rewriting the problem to include an optional test function that permits the minimization of the necessary conditions.

$$[M_p][\dot{p}] + [Q_1^\tau][u_r] + [q][u_r] + [Q_2^\tau][u_\theta] + [Q_3^\tau][u_z] = 0, \tag{17}$$

$$[M][\dot{u}_r] + [C(u_r, u_\theta, u_z)][u_r] + [c_\theta][u_\theta] - \frac{1}{Re}[Q_1][P] + [K_{rr}][u_r] + [K_{21}][u_\theta]$$
$$+[K_{22}][u_r] + [k_r][u_r] + [k_\theta][u_\theta] + [K_{31}][u_z] + [K_{33}][u_r] = 0, \quad (18)$$
$$[M][\dot{u}_\theta] + [C(u_r, u_\theta, u_z)][u_\theta] + [c_r][u_r] - \frac{1}{Re}[Q_2][P] + [K_{11}][u_\theta] + [K_{12}][u_r]$$
$$+[k_\theta][u_r] + [K_{\theta\theta}][u_\theta] + [K_{33}][u_\theta] + [K_{32}][u_z] = 0, \quad (19)$$
$$[M][\dot{u}_z] + [C(u_r, u_\theta, u_z)][u_z] - \frac{1}{Re}[Q_3][P] + [K_{11}][u_z] + [K_{13}][u_r] -$$
$$[k_3][u_r] - [k_1][u_z] + [K_{22}][u_z] + [K_{23}][u_\theta] + [K_{zz}][u_z] = 0. \quad (20)$$

Such that all the definitions of the matrices are:

mass matrix:

$$[M] = \int_{\Omega^e} \psi\psi^\tau d\Omega = \int_{A^e}\int_0^{2\pi} [N][H][H^\tau][N^\tau] r d\theta dA = 2\pi \int_{A^e} [N][H][N^\tau][H^\tau] r dA,$$

where,

$$r_m = \frac{r_1+r_2+r_3}{3}, z_m = \frac{z_1+z_2+z_3}{3}.$$

Thus,

$$[M] = 2\pi r_m [N][H][H^\tau][N^\tau] \int_{A^e} A = 2\pi r_m A_{area}[N][H][H^\tau][N^\tau], \quad (21)$$
$$[M_p] = 2\pi r_m A_{area} \frac{1}{\beta_{ac}}[E][E^\tau]. \quad (22)$$

Moreover, the taken from style of form functions may be mentioned, like:

$$\frac{\partial\psi}{\partial r} = [N]\frac{\partial[H]}{\partial r} = [N][B][E],$$
$$\frac{\partial\psi}{\partial\theta} = 0,$$
$$\frac{\partial\psi}{\partial z} = [N]\frac{\partial[H]}{\partial z} = [N][C][E],$$

where,

$$[B] = \frac{1}{2A_{area}}\begin{bmatrix} 2b_1 & 0 & 0 \\ 0 & 2b_2 & 0 \\ 0 & 0 & 2b_3 \\ b_2 & b_1 & 0 \\ 0 & b_3 & b_2 \\ b_3 & 0 & b_1 \end{bmatrix}, [C] = \frac{1}{2A_{area}}\begin{bmatrix} 2c_1 & 0 & 0 \\ 0 & 2c_2 & 0 \\ 0 & 0 & 2c_3 \\ c_2 & c_1 & 0 \\ 0 & c_3 & c_2 \\ c_3 & 0 & c_1 \end{bmatrix}.$$

diffusion matrix:

$$[K_{rr}] = \frac{4\pi}{Re}\int_{A^e} \mu_E [N][B]\underline{[E][E^\tau]}[B^\tau][N^\tau] r dA, \quad (23)$$
$$[K_{zz}] = \frac{4\pi}{Re}\int_{A^e} \mu_E [N][C]\underline{[E][E^\tau]}[C^\tau][N^\tau] r dA, \quad (24)$$
$$[K_{11}] = \frac{2\pi}{Re}\int_{A^e} \mu_E [N][B]\underline{[E][E^\tau]}[B^\tau][N^\tau] r dA, \quad (25)$$

$$[K_{33}] = \frac{2\pi}{Re}\int_{A^e} \mu_E[N][C]\underline{[E][E^\tau]}[C^\tau][N^\tau]rdA, \tag{26}$$

$$[K_{13}] = \frac{2\pi}{Re}\int_{A^e} \mu_E[N][B]\underline{[E][E^\tau]}[C^\tau][N^\tau]rdA, \tag{27}$$

$$[K_{31}] = \frac{4\pi}{Re}\int_{A^e} \mu_E[N][C]\underline{[E][E^\tau]}[B^\tau][N^\tau]rdA, \tag{28}$$

$$[k_r] = \frac{4\pi}{Re}\int_{A^e} \mu_E[N][H][E^\tau][B^\tau][N^\tau]rdA, \tag{29}$$

$$[k_1] = \frac{2\pi}{Re}\int_{A^e} \mu_E[N]\underline{[H][E^\tau]}[B^\tau][N^\tau]rdA, \tag{30}$$

$$[k_3] = \frac{2\pi}{Re}\int_{A^e} \mu_E[N]\underline{[H][E^\tau]}[C^\tau][N^\tau]rdA, \tag{31}$$

$$[K_{\theta\theta}] = 0, [K_{22}] = 0, [K_{12}] = 0, [K_{21}] = 0, [K_{23}] = 0, [K_{32}] = 0, [k_2] = 0, [k_\theta] = 0.$$

gradient matrix:

$$[Q_1] = 2\pi r_m A_{area}[N][B]\underline{[E][E^\tau]}, \tag{32}$$

$$[Q_3] = 2\pi r_m A_{area}[N][C]\underline{[E][E^\tau]}, \tag{33}$$

$$[q] = 2\pi r_m A_{area}\underline{[E][H^\tau]}[N^\tau], \tag{34}$$

$$[Q_2] = 0.$$

convective matrix:

$$[C_r(u_r)] = 2\pi r_m A_{area}[N]\underline{[H][H^\tau]}[N^\tau][u_r]\underline{[E^\tau]}[B^\tau][N^\tau], \tag{35}$$

$$[C_z(u_z)] = 2\pi r_m A_{area}[N]\underline{[H][H^\tau]}[N^\tau][u_z]\underline{[E^\tau]}[C^\tau][N^\tau], \tag{36}$$

$$[C_\theta] = 2\pi r_m A_{area}[N]\underline{[H][H^\tau]}[N^\tau][u_\theta]\underline{[H^\tau]}[N^\tau], \tag{37}$$

$$[C_r] = 2\pi r_m A_{area}[N]\underline{[H][H^\tau]}[N^\tau][u_\theta]\underline{[H^\tau]}[N^\tau], \tag{38}$$

$$[C_\theta(u_\theta)] = 0.$$

The fact that the actual test in the now case is the indirect item that needed a well-done solution. To address this indirect item of equations (17)-(20), the Newton-Raphson technique is used. As the score, the order of the equation is going to be supplanted through the coming equation:

$$\begin{bmatrix} M & 0 & 0 & 0 \\ 0 & M & 0 & 0 \\ 0 & 0 & M & 0 \\ 0 & 0 & 0 & M_p \end{bmatrix}\begin{bmatrix} \dot{u}_r \\ \dot{u}_\theta \\ \dot{u}_z \\ \dot{p} \end{bmatrix}\begin{bmatrix} \frac{\partial R_1}{\partial u_r} & \frac{\partial R_1}{\partial u_\theta} & \frac{\partial R_1}{\partial u_z} & \frac{\partial R_1}{\partial P} \\ \frac{\partial R_2}{\partial u_r} & \frac{\partial R_2}{\partial u_\theta} & \frac{\partial R_2}{\partial u_z} & \frac{\partial R_2}{\partial P} \\ \frac{\partial R_3}{\partial u_r} & \frac{\partial R_3}{\partial u_\theta} & \frac{\partial R_3}{\partial u_z} & \frac{\partial R_3}{\partial P} \\ \frac{\partial R_4}{\partial u_r} & \frac{\partial R_4}{\partial u_\theta} & \frac{\partial R_4}{\partial u_z} & \frac{\partial R_4}{\partial P} \end{bmatrix}\begin{bmatrix} u_r^{n+1} - u_r^n \\ u_\theta^{n+1} - u_\theta^n \\ u_z^{n+1} - u_z^n \\ p^{n+1} - P^n \end{bmatrix} = -\begin{bmatrix} R_1 \\ R_2 \\ R_3 \\ R_4 \end{bmatrix}, \tag{39}$$

$$[M]\dot{U} + [S(U)] \triangle U = -[R]. \tag{40}$$

Boundary conditions (BCs): To complete the setting of the problem, we need to define the boundary conditions that are imposed on the surface of the straight channel. Homogeneous Dirichlet *BCs* are applied on the top and bottom of the channel, where the axial and radial velocities are zero on the top wall, with vanishing radial velocity only on the axisymmetric line. Since we are dealing with the laminar flow, the Poiseuille (*Ps*) flow is applied at the inlet of the channel.

4. Results

The numerical results obtained using the *GFE-AC*-method focused mainly on the impact of different parameters of the inelastic model under consideration. Particularly, the focus here is on the effect of power index (n), constant for the fluid (λ), and Reynolds number (*Re*).

***n*-variation:** Figure 1 (a) shows the cross-channel axial velocity, while 1 (b) depicts pressure along the centerline of the channel in extension thinning for fixed $\{\mu_0 = 1, k = 1, Re = 100, \lambda = 15, \beta_{ac} = 100\}$. For the axial velocity, we detected that it maintained its behavior as a Poiseuille (*Ps*) flow until reaching steady state, with a slight increase in the case of a decrease in $n < 1$. On the other hand, increased pressure can enhance the flow of extension-thinning fluids by reducing viscosity, thereby allowing for easier movement through systems. Accordingly, from the pressure profile, one can see that a decrease in the level of power-index (n)leads to a raise in the pressure due to the dominant extension-thinning influence. For example, the profile gives an increase in pressure of O(35%) from $n = 0.8$ to $n = 0.2$, O(30%) from $n = 0.8$ to $n = 0.4$, and O(22%) from $n = 0.8$ to $n = 0.6$. In addition, Figure 1c reflects the effect power index on the viscosity again in the case of extension-thinning ($n < 1$). The results demonstrated that as n decreases, the level of viscosity decreases, with a noticeable rise at $n = 0.8$, due to the thinning effect. Also, one can see that the peak in the viscosity always occurs at the center of the channel.

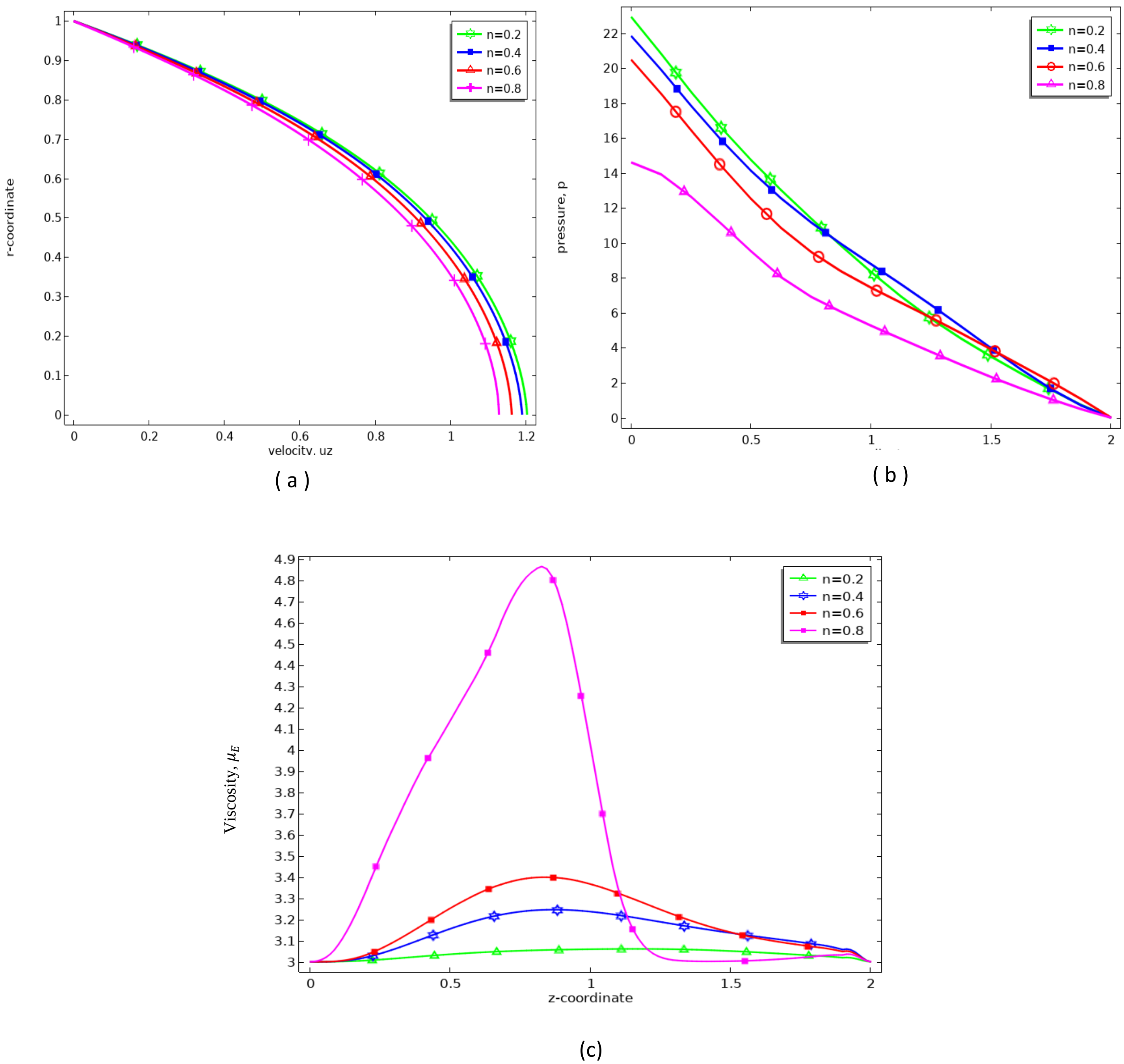

Figure 1: Axial velocity, pressure and viscosity; n-variation, $\mu_0 = 1$, $k = 1$, *Re=100*, *λ=15*, $\beta_{ac} = 100$.

***k*-variation:** The fluid may flow more consistently when the consistency parameter (k) is raised, which lowers losses from turbulence and undulations. A high consistency parameter may also help to decrease surface effects and improve flow stability because of the compact dimensions, which would enable higher velocity. From Figure 2(a-b) and with the same setting of parameters that are usually used, one can observe that the effect of the consistency index (k) was very modest on both velocity and pressure. Furthermore, Figure 2c illustrates the behaviour of viscosity under k-variation. The profiles reveal that a reduction in k results in an increase in the level of viscosity.

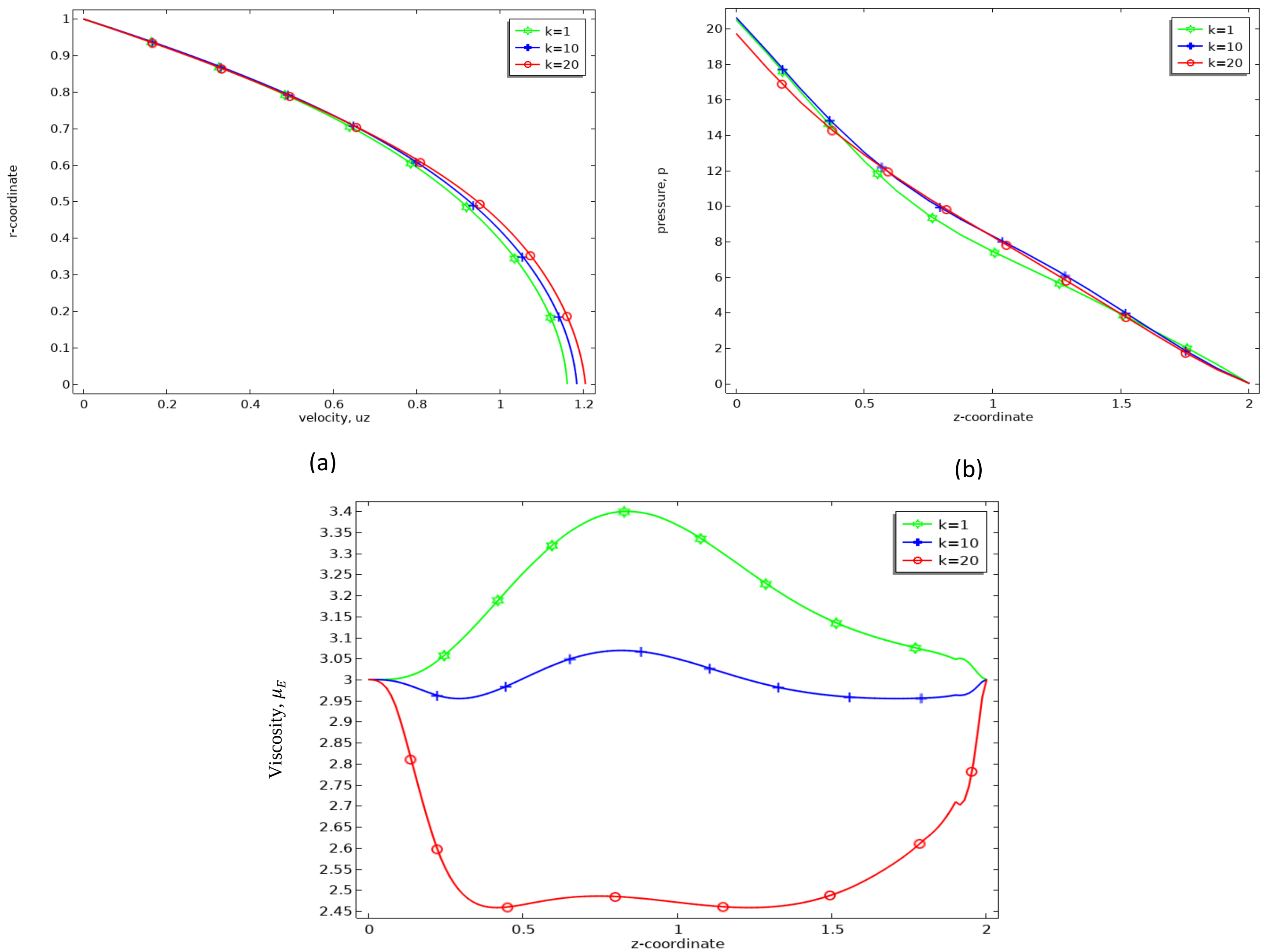

(a) (b)

(c)

Figure 2: Axial velocity, pressure and viscosity with k-variation, $\mu_0 = 1$, *Re=100*, *n=0.6*, λ *=15*,

***Re*-variation:** The effect of Reynolds number (*Re*) on the velocity is presented in Figure 3 with {μ_0 = 1, *k* = 1, *n*=0.6, λ=15, β_{ac}=100}. In laminar flow through a channel, the velocity profile is parabolic with faster near the center and decreases gradually to zero at the channel wall due to the no-slip condition. Here, as anticipated, results show that increasing *Re* causes a significant rise in the level of maximum velocity.

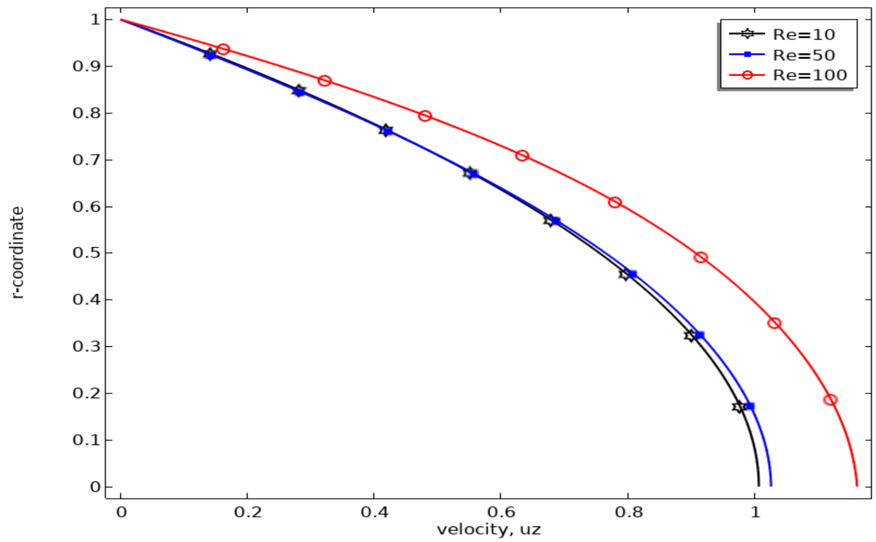

Figure 3: Velocity profiles with *Re*-variation, μ_0 = 1, *k* = 1, *n=0.6*, λ=*15*, $\beta_{ac} = 100$.

λ-variation: In the case of extension-thinning flow, the cross-channel axial velocity and pressure are displayed in Figure 4 (a-b) with fixed {μ_0 = 1, *k* = 1, *Re*=100, *n*=0.6, β_{ac}=100} and λ variation {1, 10, 15, 20}. Since the inelastic parameter (λ) represents the resistance to fluid flow between two surfaces in contact. Accordingly, a very slow change in velocity is observed as the inelastic parameter(λ) increases. In addition to maintaining the flow rate, the same behavior has occurred for pressure, where a significant decrease in pressure level has appeared as the inelastic parameter (λ) increased.

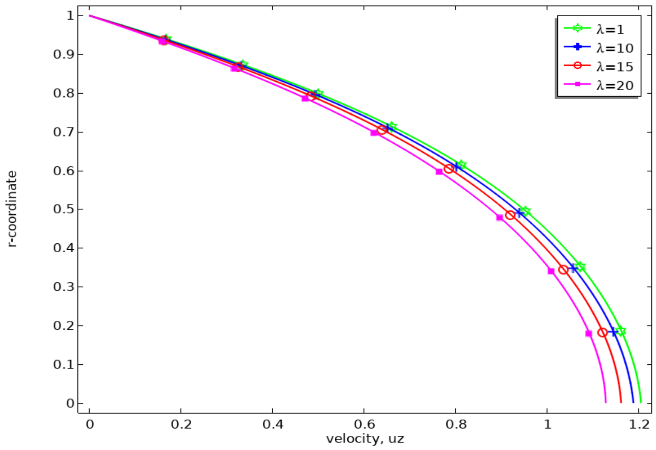

(a)

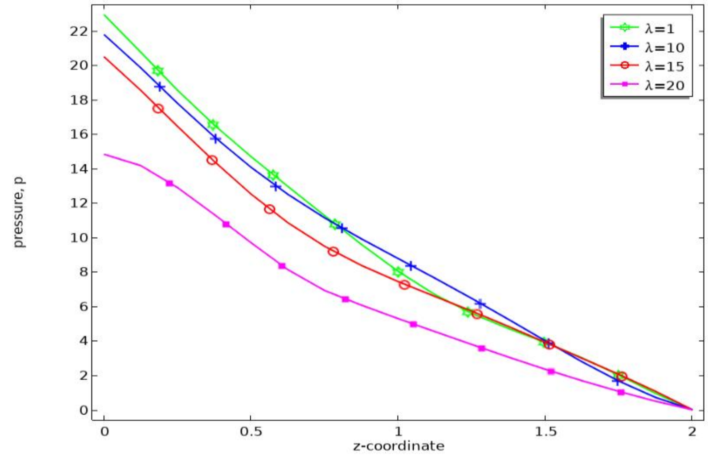

(b)

Figure 4: Axial velocity and pressure with λ-variation, μ_0 = 1, k = 1, n=0.6, Re=100, β_{ac} = 100 .

β_{ac}**-variation:** The effect of the artificial compressibility parameter {β_{ac}=10, 50, 80, 100}with fixed {μ_0 = 1, k = 1, n=0.6, Re=100, λ = 15 } on the level of axial velocity and pressure is presented in Figure 5(a-b). The axial velocity profile is plotted at z=1.5 (Figure 5a), while along the centerline was the plotting of pressure (Figure 5a). From observing the results, we found that there is a different influence of β_{ac} on both axial velocity and pressure, as the effect of the parameter is directly proportional to velocity and inversely proportional to pressure. The reason for this is due to a fluid moving more swiftly when artificial compressibility is applied because the pressure pushes the fluid molecules, and the flow rate rises because of the fluid molecules moving more quickly. Additionally, in order to optimize fluid flow and establish a dynamic equilibrium for steady flow, artificial compressibility causes the natural pressure inside the cylinder to be modified. There is also an interesting point and striking observation that was made in the pressure value at β_{ac}=10, which is that the pressure value at the region close to the inlet of the channel is less than the level of the other values, and then it begins to gradually increase after the first quarter of the channel to take the general situation consistent with the results. Moreover, the impact of β_{ac} on the viscosity through a straight line parallel to the axisymmetric line is presented as well in Figure 5c with the same setting of parameters. The comparative plots show that there is a significant effect on viscosity with a small β_{ac}=10, after, which the differences drop away with a gradual decrease observed when the

β_{ac} −value increases to take close values of about 3 units. For instance, one can observe that a reduction in the level of viscosity of O(77%) from β_{ac}=10 to β_{ac}=100 has occurred.

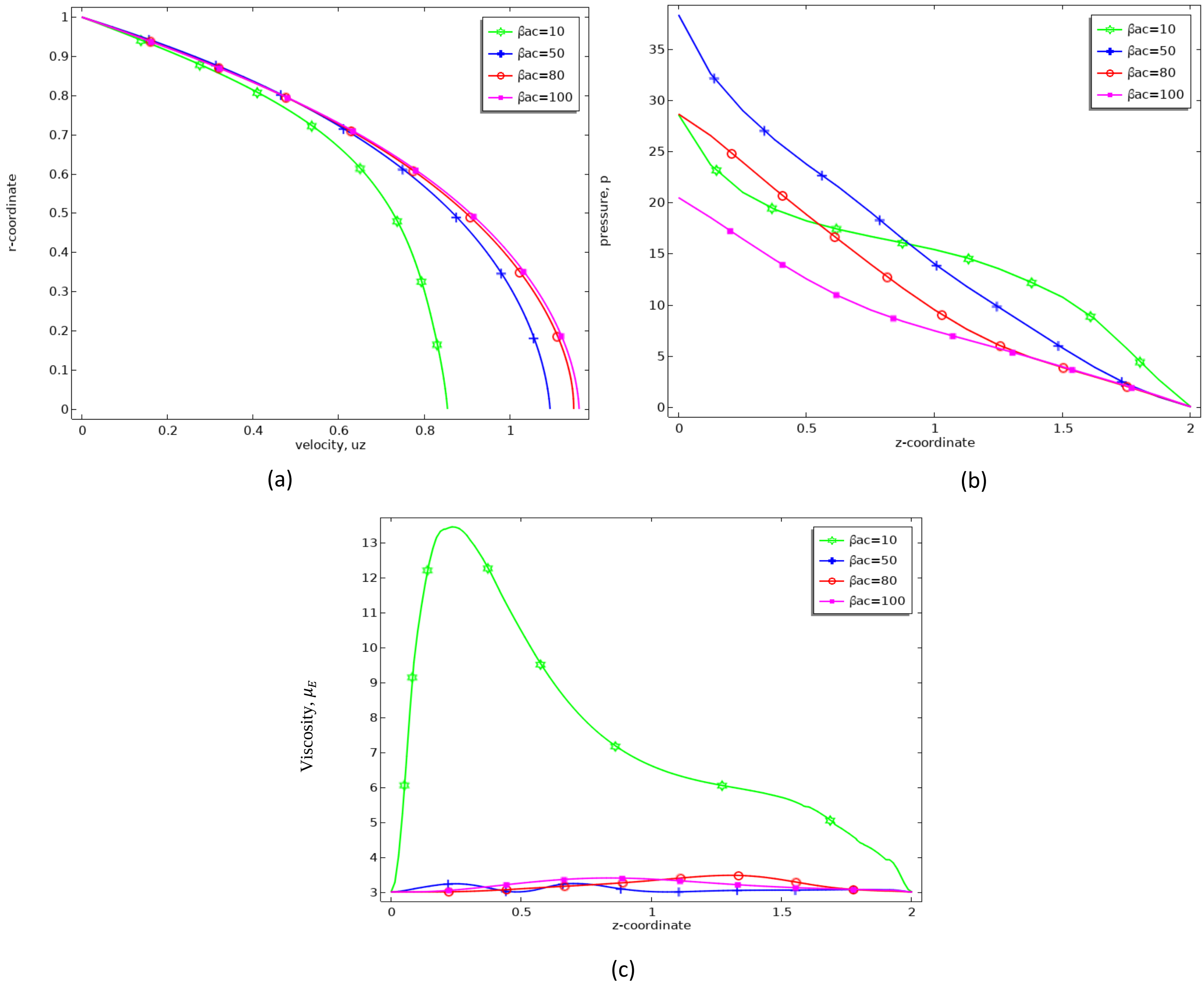

Figure 5: Axial velocity, pressure and viscosity with β_{ac}-variation, $\mu_0 = 1$, $k = 1$, *n=0.6*, *Re=100*, $\lambda = 15$.

5. Conclusions

In this study, a numerical simulation of an inelastic and incompressible fluid is conducted utilizing the Galerkin finite element method in a cylindrical coordinate system. The numerical method is employed based on the artificial compressibility approach to facilitate the conversion process of the incompressible continuity equation from the elliptic equation to a hyperbolic compressible equation by adding the artificial compressibility factor to the continuity equation is the method. This change makes it possible to handle numerical solutions with greater flexibility and helps to prevent the issues brought on by stiff situations. The impact of Reynolds number (*Re*), power index (*n*), consistency coefficient (*k*), artificial compressibility coefficient (β_{ac}), and λ on the behavior of solution components is tested. The results show the effect of extension-thinning on the solutions.

References

[1] R. P. Bharti, R. P. Ram, A. K. Dhiman, Computational analysis of cross-flow of power-law fluids through a periodic square array of circular cylinders, Asia-Pacific J Chem. Eng.,17 (2022) e2748, **https://doi.org/10.1002/apj.2748**

[2] S. Karimi, M. Dabagh, P. Vasava, M. Dadvar, B. Dabir, P. Jalali, Effect of rheological models on the hemodynamics within human aorta: Cfd study on ct image-based mgeometry, J. Nonnewton. Fluid Mech., 207 (2014) 42-52, https://doi.org/10.1016/j.jnnfm.2014.03.007

[3] C. Carer, L. X. Driever, S. Kobben, M. Mckenzie, F. Rhenman, O. V. d. Sype, J.V.D. Toorn, C. V.Wezel, C. M. d. A. Veiga, A. Vinarskis, et al., Effect of parameter variation on the viscosity of ethanol gel propellants, J Aerospace Tech. Manage., 13 (2021) e1121, https://doi.org/10.1590/jatm.v13.1196

[4] J. Boyd, J. M. Buick, S. Green, Analysis of the casson and carreau-yasuda non newtonian blood models in steady and oscillatory flows using the lattice Boltzmann method, Phys. Fluids, 19 (2007), https://doi.org/10.1063/1.2772250

[5] D. Liepsch, S. Sindeev, S. Frolov, An impact of non-Newtonian blood viscosity on hemodynamics in a patient-specific model of a cerebral aneurysm, J Phys: Conference Series, IOP Publishing, 2018, p.012001, https://doi:10.1088/1742-6596/1084/1/012001

[6] D. Binding, A. Blythe, S. Gunter, A. Mosquera, P. Townsend, M. Webster, Modelling polymer melt flows in wirecoating processes, J. Nonnewton. Fluid Mech., 64 (1996) 191-206, https://doi.org/10.1016/0377-0257(96)01447-4

[7] B. Debbaut, M. Crochet, Extensional effects in complex flows, J Nonnewton Fluid Mech., 30 (1988) 169-184, https://doi.org/10.1016/0377-0257(88)85023-7

[8] I. Mutlu, P. Townsend, M. Webster, Simulation of cable-coating viscoelastic flows with coupled and decoupled schemes, J Nonnewton Fluid Mech., 74(1998)1-23, https://doi.org/10.1016/S0377-0257(97)00069-4

[9] Alaa Abdulwahid Sharhan, A. H. A. Al-Muslimawi, Numerical Study of Shear and Extensional Inelastic Contraction Flows, CFD Letters 15 (2023) 107-121, https://doi.org/10.37934/cfdl.15.8.107121

[10] P. A. Madsen, H. Schäffer, A discussion of artificial compressibility, Coastal Eng., 53 (2006) 93-98, https://doi.org/10.1016/j.coastaleng.2005.09.020

[11] R. Peyret , T.D. Taylor, Computational Methods for Fluid Flow, New York: Springer Verlag, 1983, https://doi.org/10.1007/978-3-642-85952-6

[12] P.-H. Kao, R.-J. Yang, A segregated-implicit scheme for solving the incompressible Navier-stokes equations, Comp. Fluids, 36(2007) 1159-1161, https://doi.org/10.1016/j.compfluid.2006.11.001

[13] J. Chang, D. Kwak, On the method of pseudo compressibility for numerically solving incompressible flows, in: 22nd Aerospace Sciences Meeting, 1984, p. 252, https://doi.org/10.2514/6.1984-252

[14] D. Choi, C. L. Merkle, Application of time-iterative schemes to incompressible flow, AIAA J, 23(1985) 1518-1524, https://doi.org/10.2514/3.9119

[15] B. K. Jassim, A. H. Al-Muslimawi, Numerical analysis of newtonian flows based on artificial compressibility ac method, Journal of Al-Qadisiyah Comp. Sci. Math., 9 (2017) 115-128, https://doi.org/10.29304/jqcm.2017.9.2.303

[16] R. Y. Yasir, A. H. Al-Muslimawi, B. K. Jassim, Numerical simulation of non-Newtonian inelastic flows in channel based on artificial compressibility method, Journal of Applied and Comput. Mech..,6 (2020) 271-283, https://DOI: 0.22055/JACM.2019.29948.1650

[17] J. R. Abdul-Jabbar, A. H. Al-Muslimawi, I. A. Fadhel, Computational study of the flow of newtonian fluid through a straight channel and lid-driven cavity, Iraqi J Sci., 64(2023) 4043-4057, https://DOI: 10.24996/ijs.2023.64.8.28

[18] A. Al-Haboobi, G. A. Al-Juaifri, A. H. Al-Muslimawi, Numerical study of newtonian laminar flow around circular and square cylinders, Results Control Optim., 14 (2024) 100328, https://doi.org/10.1016/j.rico.2023.100328

دراسة عددية لتدفق السوائل غير المرنة المتمددة-المرققة: طريقة العناصر المحدودة لغالركين

احمد جبار غانم و علاء حسن عبد الله

قسم الرياضيات- كلية العلوم – جامعة البصرة

المستخلص

في هذا البحث، نُجري محاكاةً لتدفق السوائل غير المرنة بالتمدد والترقق عبر قناة مستطيلة محورية التناظر. ولوصف حركة السوائل، تُستخدم عادةً معادلات التفاضل الجزئي لحفظ الكتلة وحفظ الزخم. وتُقدم هذه الدراسة هذه المعادلات في سياق نظام الإحداثيات الأسطواني . والنقطة الأساسية هنا هي ضرورة تعريف اللزوجة كمتغير، مما يتطلب إدخال معادلة تأسيسية إضافية. وبناءً على ذلك، يُقدم نموذج غير مرن بالتمدد والترقق، يسمى SI-Fit-II لمعالجة حالة اللزوجة . وفي هذه الدراسة، تُطبق طريقة العناصر المحدودة لغالركين، لقائمة على طريقة الضغط الاصطناعي . ولتلبية تحليل الطريقة، يُستخدم تدفق بوازوي على طول قناة دائرية في حالة متساوية الحرارة كمسألة اختبار بسيطة. ويُجرى هذا الاختبار بأخذ مقطع دائري من الأنبوب. تمت مناقشة تأثير العديد من المعلمات، مثل معامل الاتساق ومؤشر القدرة للنموذج، ومعامل الانضغاط الاصطناعي β_{ac} ،ورقم رينولدز Re . يُجرى هذا الاختبار بأخذ مقطع دائري من الأنبوب .